

# BS 196: an old star cluster far from the SMC main body<sup>\*</sup>

E. Bica<sup>1</sup>†, J. F. C. Santos Jr.<sup>2</sup> and A. A. Schmidt<sup>3</sup>

<sup>1</sup>*Departamento de Astronomia, Universidade Federal do Rio Grande do Sul, Av. Bento Gonçalves 9500, Porto Alegre 91501-970, RS, Brazil*

<sup>2</sup>*Departamento de Física, ICEx, Universidade Federal de Minas Gerais, Av. Antônio Carlos 6627, Belo Horizonte 31270-901, MG, Brazil*

<sup>3</sup>*Departamento de Matemática, Universidade Federal de Santa Maria, Av. Roraima 1000, Santa Maria 97105-900, RS, Brazil*

Accepted 2008 September 10. Received 2008 August 26; in original form 2008 July 3

## ABSTRACT

We present *B* and *V* photometry of the outlying SMC star cluster BS 196 with the 4.1-m SOAR telescope. The photometry is deep (to  $V \approx 25$ ) showing  $\approx 3$  mag below the cluster turnoff point (TO) at  $M_V = 2.5$  ( $1.03 M_\odot$ ). The cluster is located at the SMC distance. The colour-magnitude diagram (CMD) and isochrone fittings provide a cluster age of  $5.0 \pm 0.5$  Gyr, indicating that this is one of the 12 oldest clusters so far detected in the SMC. The estimated metallicity is  $[Fe/H] = -1.68 \pm 0.10$ . The structural analysis gives by means of King profile fittings a core radius  $R_c = 8.7 \pm 1.1$  arcsec ( $2.66 \pm 0.14$  pc) and a tidal radius  $R_t = 69.4 \pm 1.7$  arcsec ( $21.2 \pm 1.2$  pc). BS 196 is rather loose with a concentration parameter  $c = 0.90$ . With  $M_V = -1.89 \pm 0.39$ , BS 196 belongs to the class of intrinsically fainter SMC clusters, as compared to the well-known populous ones, which starts to be explored.

**Key words:** Magellanic Clouds – galaxies: star clusters

## 1 INTRODUCTION

Luminous old SMC star clusters (we will refer as such to the red SMC clusters with age  $> 1$  Gyr – including intermediate age clusters (IAC) to globular clusters) have been systematically observed in the last decade, using mainly  $CT_1$  photometry at CTIO (e.g. Piatti et al. 2001, 2007), and Hubble photometry with different cameras (e.g. Mighell, Sarajedini & French 1998; Glatt et al. 2008). The age and age-metallicity distributions in these studies reveal essential features of the star formation history of the SMC system. Any new star cluster added to these distributions provides fundamental pieces of information to them.

The star cluster BS 196 was discovered on Sky Survey plates and first reported by Bica & Schmitt (1995). It was also listed by Bica & Dutra (2000) in a update of the SMC catalogue. Recently, two star clusters from Bica & Schmitt’s catalogue were found to be old SMC clusters. The 4.3 Gyr old (Sabbi et al. 2007) cluster BS 90 is unique, being projected inside the large H II region complex NGC 346 and BS 121 with 2.3 Gyr (Piatti et al. 2005) is projected on the SMC main body.

BS 196 appears to be a less populous cluster on the Sky Survey plates, with a diameter somewhat smaller than 1 arcmin. It is located at  $\alpha_{2000} = 1h48m02s$  and  $\delta_{2000} = -70^\circ 00' 15''$ . It is projected  $5.1^\circ$  to the Northeast of the SMC

bar and the optical centre at  $\alpha_{2000} = 00h52m45s$ ,  $\delta_{2000} = -72^\circ 49' 43''$  (Crowl et al. 2001), being one of the angularly farthest SMC clusters known (Bica & Schmitt 1995). It is more distant from the bar than Lindsay 1, an extreme cluster to the West, together with AM-3 (Bica & Schmitt 1995). It is fundamental to carry out deep photometry of the cluster BS 196 to unveil its nature, whether associated to the SMC or a far globular cluster in the Galactic halo.

This paper is organized as follows. In Sect. 2 *BV* photometry of BS 196 obtained with the SOAR telescope is presented. In Sect. 3 we determine the cluster astrophysical parameters by means of Padova isochrone fittings, finding that it belongs to the SMC. In Sect. 4, cluster structural properties are derived. In Sect. 5 we discuss the cluster age and metallicity in the context of the SMC enrichment and star formation histories. Concluding remarks are given in Sect. 6.

## 2 OBSERVATIONS

The SOAR optical imager (SOI) mounted in a bent-Cassegrain configuration to the 4.1-m SOAR telescope (Cerro Pachón, Chile) was employed to observe BS 196 in service mode. Images taken with Bessel *BV* filters were obtained on the photometric night of 2007 November 11, using the SOI mini-mosaic of two E2V 2x4k CCDs (1 pixel =  $15 \mu\text{m}$ ) to cover a 5.2 arcmin square field of view. The observations were carried out with the CCDs binned to 2x2 pixels to yield a scale of 0.154 arcsec/pixel. The readout mode

<sup>\*</sup> Based on observations made with the SOAR 4.1-m telescope (proposal SO2007B-007)

† E-mail: bica@if.ufrgs.br

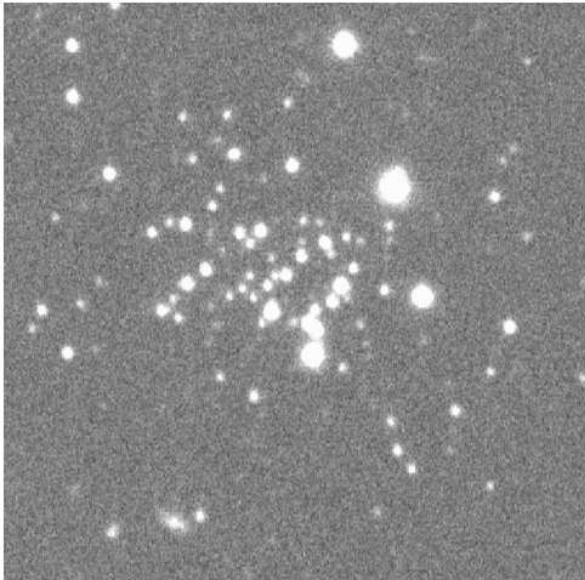


**Figure 1.** SOI  $V$  image extraction of BS 196 field. North is up and East to the left. The field dimensions are  $1.2 \times 1.2$  arcmin<sup>2</sup>.

was set to *fast* (readout noise  $4.1 e^-$ ) and the gain was  $1.9 e^- \text{ADU}^{-1}$ . The seeing FWHM was  $\sim 0.95$  arcsec in  $B$  and  $\sim 0.8$  arcsec in  $V$  with the observations being taken at airmass 1.31. Two images in each filter were obtained, with single exposure times of 480 s in  $B$  and 195 s in  $V$ . The telescope pointing was so as to carefully center the object on one of the CCDs in order to avoid the gap of 7.8 arcsec between them. The combined  $V$  image of BS 196 is shown in Fig. 1, as an extraction of the SOI frame.

Standard fields were also observed with airmasses bracketing the target airmass for photometric calibration. The NGC 121 Stetson’s photometric standard field<sup>1</sup> (Stetson 2000) provides  $B$  and  $V$  magnitudes of  $\approx 110$  stars. Since it covers a larger field than the SOI FOV, a fraction of it containing 28 stars was observed twice, with different airmasses, on the same night. Also the standard stars A, C and D in the TPhe field were observed once.

The CCD frames were reduced with IRAF software (Tody 1993). They were pre-reduced (bias/overscan subtraction, flat-field division using dome flats, trimming of overscan frame regions and transformation of MEF files into single FITS files) using SOAR scripts suited to operate on SOI images. Removal of cosmic rays was performed by combining the two exposures in each filter.

The combined  $B$  image was registered using selected star coordinates of the combined  $V$  image. Then a single list of star coordinates was generated (using  $V$  image) for all stars brighter than 5 times the sky fluctuation and their aperture photometry computed. As in the previous steps, DAOPHOT as implemented in IRAF was employed to perform point spread function (PSF) photometry. For the target cluster there was no particular difficulty in finding relatively bright, isolated stars for building the PSF model because of its location far from the SMC main body. Three stars with

**Table 1.** RMS and coefficients of transformation equations.

| $i$ | $B$                | $V$                  |
|-----|--------------------|----------------------|
| 1   | $-0.230 \pm 0.016$ | $-0.3065 \pm 0.0057$ |
| 2   | 0.25               | 0.14                 |
| 3   | $-0.480 \pm 0.099$ | $-0.384 \pm 0.046$   |
| 4   | $0.357 \pm 0.074$  | $0.376 \pm 0.034$    |
| RMS | 0.026              | 0.017                |

brightness covering those of cluster stars were chosen as PSF stars in each  $B$  and  $V$  frames. The instrumental magnitudes were obtained by running DAOPHOT task ALLSTAR. Besides those, ALLSTAR also outputs photometric quality parameters, namely,  $\chi$ , which provides the goodness of PSF fitting (ideally equal to 1), and *sharp*, which accounts for the difference between the observed width of an object and the width of the PSF model (ideally equal to zero). Only stars with  $\chi < 3.0$  and  $-0.5 < \textit{sharp} < 0.5$  were kept. The final table of magnitudes contains 660 stars. Aperture corrections of  $-0.346$  and  $-0.343$  for  $B$  and  $V$  respectively were applied to the instrumental magnitudes in order to bring those to the standard stars scale.

Given the small range of airmasses covered by the standards we did not derive extinction coefficients but use  $k_B = 0.25$  and  $k_V = 0.14$  (CTIO average) as constants in the transformation equations. The photometric calibration was accomplished by using FITPARAMS IRAF task with the following transformation equations:

$$mb = B + b_1 + b_2(X_B - 1.4) + b_3(B - V) + b_4(B - V)X_B \quad (1)$$

$$mv = V + v_1 + v_2(X_V - 1.4) + v_3(B - V) + v_4(B - V)X_V \quad (2)$$

where  $b_i$  and  $v_i$  ( $i = 1, \dots, 4$ ) are the derived coefficients,  $mb$  and  $mv$  are the instrumental magnitudes,  $B$  and  $V$  are the standard magnitudes and  $X_B$  and  $X_V$  the airmasses. Note that  $b_2 = k_B$  and  $v_2 = k_V$  and the numerical factor 1.4 were used to minimize the significance of the extinction coefficients. Also the initial zeropoint magnitude was 25.0. The fittings rms and derived coefficients are given in Table 1.

The transformation equations were then inverted and applied to the target cluster.

Photometric errors in the  $B$  and  $V$  bands are shown in Fig. 2. As a consequence of the deeper image in  $B$ , the errors are smaller in  $B$  than in  $V$  at a same magnitude. At  $\text{mag}=24$   $\sigma_B \approx 0.05$  and  $\sigma_V \approx 0.10$ .

### 3 COLOUR-MAGNITUDE DIAGRAM AND ASTROPHYSICAL PARAMETERS

We indicate in Fig. 3 a series of concentric spatial regions selected for building  $V \times (B - V)$  CMDs.

The CMDs are shown in Fig. 4. The central part ( $r < 20$  arcsec) shows a clear main sequence (MS) and giant branch (GB). In the outer rings to as far as  $r < 40$  arcsec the MS can still be traced.

Before fitting isochrones to the cluster inner region CMD, we searched the literature for values of reddening and distance modulus aiming at constraining their ranges in the process. The reddening was taken from HI (Burstein & Heiles 1982) and dust

<sup>1</sup> <http://www3.cadc-ccda.hia-ihp.nrc-cnr.gc.ca/community/STETSON/standards>

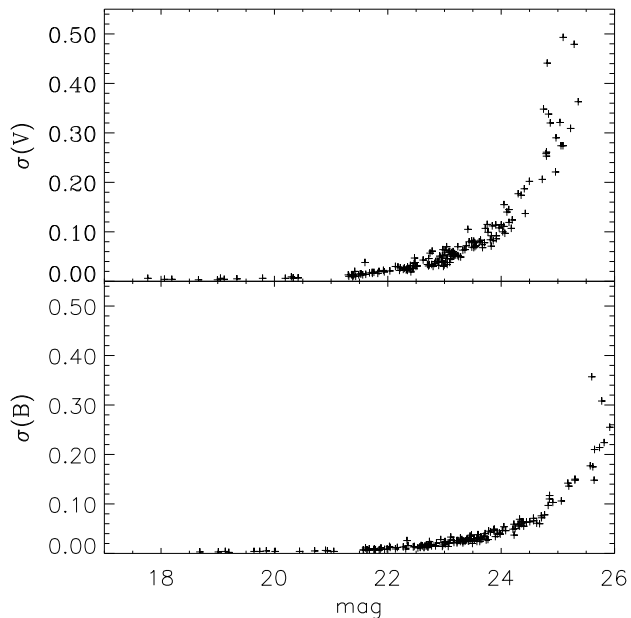


**Figure 2.** Photometric errors in  $B$  (lower panel) and  $V$  (upper panel) as a function of the respective magnitude. The data are limited to errors smaller than 0.5 and cover an area about 4 times the cluster visual area ( $r = 130$  pix), centred in the cluster.

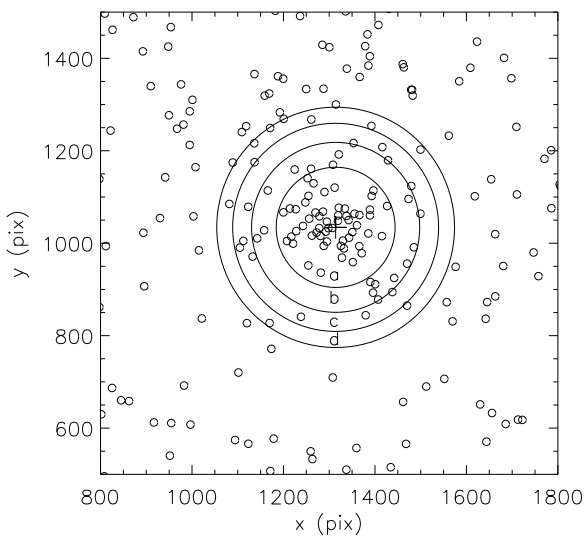


**Figure 3.** Spatial distribution of stars in the field of BS 196, where the cluster centre (plus symbol) and the annular regions used to build the CMDs of Fig. 4 are shown (a, b, c and d). The field size is  $150 \times 150$  arcsec<sup>2</sup>. North is up and East to the left.

(Schlegel, Finkbeiner & Davis 1998) maps. For the cluster galactic coordinates ( $l = 295.98^\circ$ ,  $b = -46.35^\circ$ ) both maps agree:  $E(B - V) = 0.02 \pm 0.01$  (Burstein & Heiles 1982) and  $E(B - V) = 0.024 \pm 0.004$  (Schlegel, Finkbeiner & Davis 1998), where the first value has been brought to the scale of Schlegel, Finkbeiner & Davis (1998). We adopt the mean value  $E(B - V) = 0.02 \pm 0.01$ . The distance modulus was

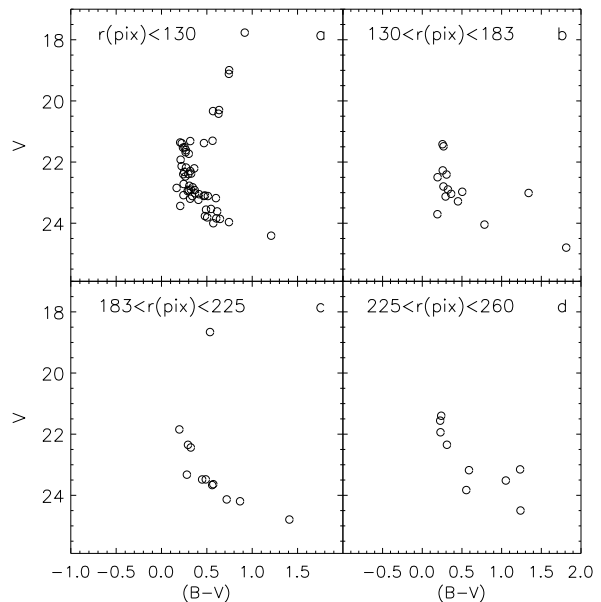


**Figure 4.** CMDs of annular regions of same area centred in the cluster. The circular inner region has the cluster visual radius (a). The boundary radius, in pixels, of outer adjacent rings are indicated (b, c, d). The panels contain data with photometric errors less than 0.5 mag.

allowed to change within  $(m-M)_\odot = 18.9 \pm 0.2$  (Westerlund 1997), where the uncertainty accounts for the SMC line-of-sight depth (Crowl et al. 2001).

Fortunately the cluster presents a well populated TO and well defined giant (RGB) and subgiant (SGB) branches owing to the accurate photometry in this uncontaminated field, which helps further to narrow down the uncertainties associated with isochrone fitting. Due to the presence of giants, we do not identify any degeneracy yielded by combinations of reddening, distance modulus, age and metallicity since each of these parameters have a different effect on the isochrones. Considering the domain of ages dealt with in the present study, the main parameters shaping an isochrone are its age (affects principally the TO) and its metallicity (affects principally the RGB but also the TO). On the other hand, reddening and distance modulus are related to displacement of data and isochrones in the CMD plane. A certain combination of reddening and distance modulus applied to the data matches them with a selected isochrone in the CMD plane.

The procedure employed to find the best representative isochrones of the cluster CMD was interactive:

- (i) we used data of the inner region of the cluster ( $r < 20$  arcsec) with photometric errors below 0.1 mag.
- (ii) the initial values  $E(B - V) = 0.02$  and  $(m-M)_\odot = 18.9$ , as justified above, were then applied to the data.
- (iii) we then visually chose Padova isochrones (Girardi et al. 2002) which best matched the corrected data in the CMD. A good match was achieved by using the isochrone with  $\log t = 9.7$  and  $Z = 0.0003$ , by revising to  $(m-M)_\odot = 18.95$  the distance modulus correction applied to the data and by keeping the initial reddening,  $E(B -$

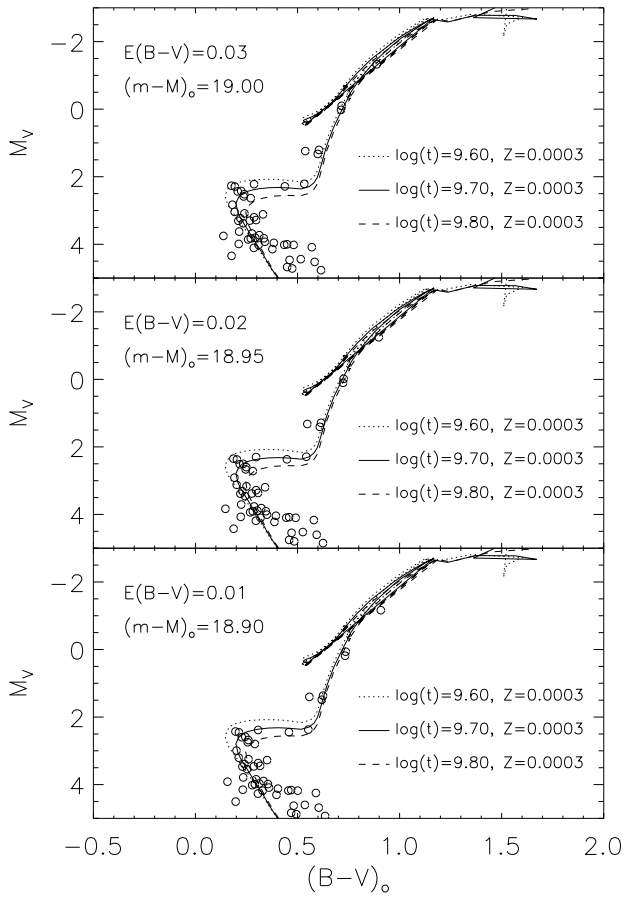


**Figure 5.** Isochrone fitting to the cluster CMD inner region. Stars with photometric errors above 0.1 mag have been excluded. The three panels show the effect of different reddening and distance modulus applied to the data. Each panel contains the same set of Padova isochrones of  $Z=0.0003$  and different ages.

$V)=0.02$ . Although this distance modulus places the cluster slightly farther than that derived from a series of clusters (Crowl et al. 2001), namely  $(m-M)_0=18.77$ , we conclude that BS 196 appears to be located at the SMC distance.

(iv) in order to account for the uncertainties in age, additional isochrones of  $\log t = 9.6, 9.8$  and  $Z=0.0003$  were superimposed in the CMD to the data corrected for the extreme and average values that reddening and distance modulus may assume due to errors of 0.01 mag and 0.05 mag, respectively. Fig. 5 shows this step. Considering that the three isochrones encompass the data, producing reasonable fits whenever the errors in  $E(B-V)$  and  $(m-M)_0$  are taken into account, the adopted age is the average  $\log t = 9.70 \pm 0.04$  ( $5.0 \pm 0.5$  Gyr), which comes from assigning weight two to the central isochrone and weight one to the marginal ones.

(v) the cluster metallicity was derived by matching isochrones of age  $\log t = 9.70$  and different metallicities to the data which was corrected for  $(m-M)_0 = 18.95$  and  $E(B-V) = 0.02$ . These fittings are shown in Fig. 6 for isochrones with  $Z=0.0001, 0.0003, 0.0005, 0.0007$ . They provide the stellar mass in the TO region:  $1.03 M_\odot$ . In a procedure similar to that used for age determination, an average metallic-

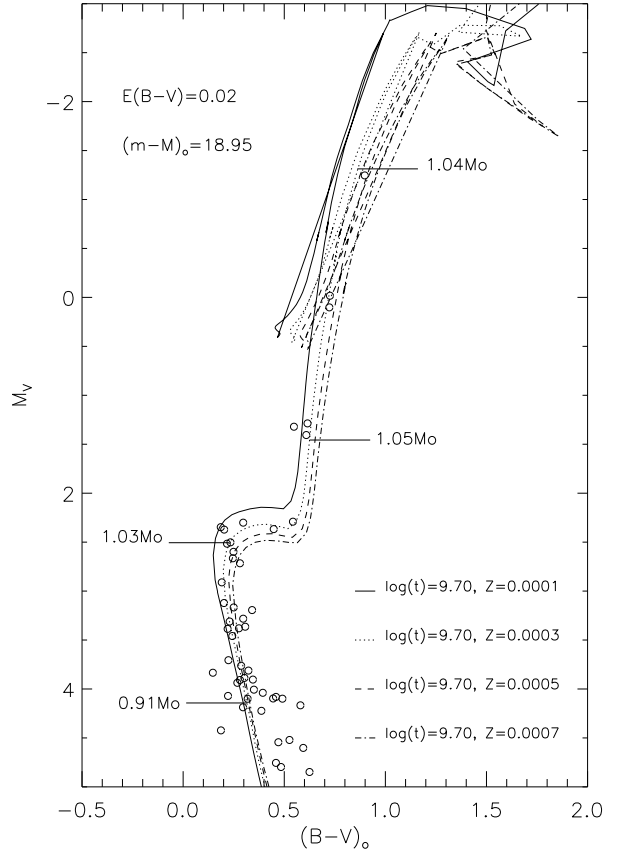


**Figure 6.** Isochrone fitting to the cluster CMD inner region. Stars with photometric errors above 0.1 mag have been excluded. The data have been corrected by the best achieved values of reddening and distance modulus. The effect of different isochrone metallicities for the best fitted age is shown. Stellar masses in specific isochrone loci are also indicated.

ity of  $Z=0.00040 \pm 0.00009$  ( $[Fe/H]=-1.68 \pm 0.10$ ) was derived by assigning weight two to the central two isochrones ( $Z=0.0003$  and  $Z=0.0005$ ), given that both seem to represent equally well the overall stars loci in the CMD and weight one was assigned to the marginal isochrones ( $Z=0.0001$  and  $Z=0.0007$ ), which encompass most of the stars brighter than 1 mag below the TO.

The Padova isochrones have a widespread use and are successful in reproducing the stars loci in CMDs of stellar clusters found in nature. However, debate on specific details of stellar evolution (e. g. convective overshooting) have not been settled to a consensus among the groups that build the stellar evolutionary models. To evaluate the effect of using different sets of isochrones on the astrophysical parameters derived for BS 196, we compare in Fig. 7 Padova isochrones with those of  $Y^2$  (Yi 2001) of similar properties. Fig. 7a compares isochrones of  $Z=0.0003$  and different ages, showing an overall resemblance for similar age isochrones. Slight differences occur in the TO region in the sense that  $Y^2$  isochrones of same age are brighter and bluer than the Padova isochrones, the effect being less relevant for older ages. Fig. 7b presents isochrones of  $\log t = 9.70$  and different metallicities, again showing the overall similarities between sets. Even slighter loci differences are seen as an effect of

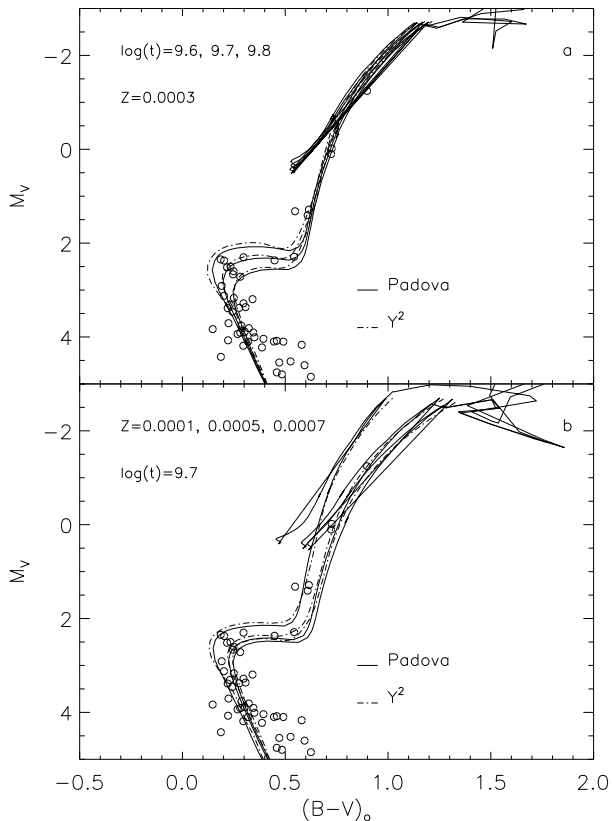


**Figure 7.** Comparison of Padova and  $Y^2$  isochrones for the interval of age and metallicity investigated in the present work. The data is the same of Fig. 6. (a) Effect of changing age at  $Z=0.0003$ ; (b) Effect of changing metallicity at  $\log t=9.70$ .

metallicity as compared to that on age. The small differences are in the sense that  $Y^2$  isochrones are brighter and bluer than the Padova isochrones of same metallicity. All these slight isochrone differences are within our errors determined for the cluster parameters. In summary, the close resemblance of these sets for ages around 5 Gyr indicates that our estimates of age and metallicity for BS 196 does not depend on whether we choose one or another set. It is worth mentioning on this regard that Padova and  $Y^2$  isochrones are based on stellar evolutionary tracks built with different input physics and different prescriptions for conversion from the theoretical to the observational plane.

#### 4 STELLAR DENSITY PROFILE AND STRUCTURAL PARAMETERS

The first step towards the construction of a representative stellar density profile is the determination of the object centre, which was accomplished by the moment-based ellipse fitting, as described by Banks, Dodd & Sullivan (1995), to the images of the cluster. The cluster overall structure is well represented by an ellipse with centre at  $x = 1314.05 \pm 0.34$ ,  $y = 1034.34 \pm 0.24$  (pixel coordinates, see Fig. 3), ellipticity  $\epsilon = 1 - b/a = 0.27 \pm 0.05$  and position angle  $PA = (-3.07 \pm 0.61)^\circ$ .

To take into account the cluster projected elliptical shape, the radial density profile (RDP) was computed within circular rings but with the star coordinates modified by including the dependence on their position angles relative to the ellipse orientation  $PA$  and the cluster  $\epsilon$ . The procedure is similar to a deprojection of the cluster on its major axis.

We employ two-parameter (central stellar surface density,  $\sigma_0$ , and core radius,  $R_c$ ) and three-parameter ( $\sigma_0$ ,  $R_c$  and tidal radius,  $R_t$ ) King profiles (King 1962, 1966) to derive the cluster structural properties. Due to the non-populous nature of the cluster we do not use integrated fluxes, rather we employ star counts to derive radial density profiles. Besides the cluster centre given above, which corresponds to the intensity-weighted centroid, we tested a few other centres to optimize higher central counts, but the results were essentially the same.

The results of the analysis are given in Fig. 8. The cluster has a well defined profile (Fig. 8a), which indicates a limiting radius of  $47 \pm 2$  arcsec ( $14.38 \pm 0.81$  pc), determined where profile and background merge (Fig. 8b). The background has been determined by fitting a constant to the outermost 2 rings. In Fig. 8b this background is shown sided by its  $1\sigma$  dispersion. The fitted constant background was then subtracted from the overall surface density and a King-profile fitting was performed.

The fitted functions are presented in Fig. 8c and 8d in log scales together with the best fit parameters. The two-parametric King function should better represent the cluster inner regions and the three-parametric King function should provide a better estimate of the cluster overall structure. In both fittings the estimates of  $R_c$  agree within the uncertainties. The two-parametric King function gives a slightly lower value of  $\sigma_0$  than the three-parametric one. The tidal radius is well constrained in spite of the fluctuations in the density of cluster stars in its outskirts, almost at the background level. Such fluctuations (represented by poissonian errors in Fig. 7) are taken into account in the fitting by applying a weighted least-squares method.

Based on the three-parametric King function fitting, the structural parameters of BS 196 are  $\sigma_0 = 0.142 \pm 0.015$  stars.arcsec $^{-2}$  ( $1.52 \pm 0.16$  pc $^{-2}$ ),  $R_c = 8.7 \pm 1.1$  arcsec ( $2.66 \pm 0.14$  pc) and a tidal radius  $R_t = 69.4 \pm 1.7$  arcsec ( $21.2 \pm 1.2$  pc). BS 196 is rather loose with a concentration parameter  $c = 0.90$ .

In general the low mass stars do not contribute significantly to the cluster integrated light (Santos, Bica & Dottori 1990). Thus the observed stars in BS 196 lead to an estimate of the cluster integrated magnitude of  $M_V = -1.89 \pm 0.39$ , and integrated colour  $(B - V) = 0.563 \pm 0.090$ . The uncertainties account for an error of 10 per cent in the cluster visual radius.

The cluster is less luminous than AM-3 with  $M_V = -3.5 \pm 0.5$  (Da Costa 1999). Such SMC clusters are intrinsically fainter than the populous ones in both Clouds (e.g. Hodge 1960), and resemble low-mass Palomar globular clusters in the Milky Way (Bica & Bonatto 2008).

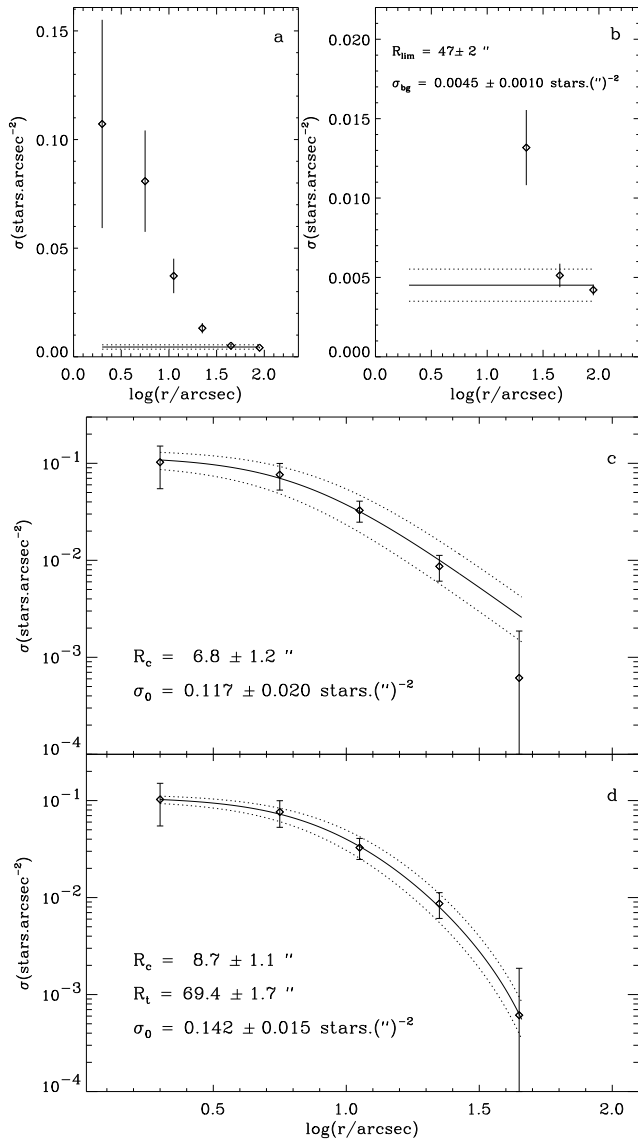


**Figure 8.** Radial density profile analysis of BS 196. (a) The RDP with poissonian error bars; (b) Zoomed version of (a) where it is determined the cluster limiting size and the constant background; The RDP in log scale with 2-parameter (c) and 3-parameter (d) King profile fittings for which central density, core and tidal radii are indicated.  $1\sigma$  dispersion for the fittings are indicated by dotted lines.

## 5 THE CLUSTER IN THE CONTEXT OF SMC EVOLUTIONARY HISTORY

In this section we compare properties of BS 196 with other SMC clusters of similar age. Rich et al. (2000) found evidence of two coeval groups of SMC clusters centred at 2 and 8 Gyr. BS 196 is located midway between the two groups.

Old SMC clusters in the following are defined as those older than the lower limit of the LMC age gap or  $\approx 4$  Gyr (Piatti et al. 2002). We indicate in Table 2 the genuine (age  $\geq 9$  Gyr) globular clusters in the SMC and intermediate age clusters (IACs) in the range 4-9 Gyr. There are 15 objects

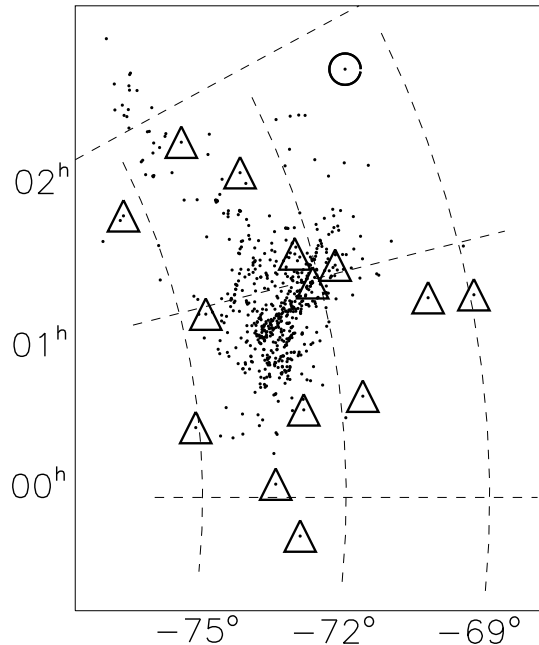


**Figure 9.** The angular distribution of the old SMC clusters (triangles) is shown together with the general population of SMC clusters (dots). BS 196 is indicated by a circle.

including the present one. Ages, metallicities and references for these clusters are given in Table 2, together with equatorial coordinates and designations (Bica et al. 2008). The BS 196 properties are included.

In Fig. 9 the angular distribution of the clusters is given overlaid on the general population of SMC clusters (Bica et al. 2008). BS 196 is another outer cluster that fits the SMC axial ratio 1:2 projected on the sky (Crowl et al. 2001). It is the only cluster located in a region otherwise clear of known old clusters. The projected distribution of old clusters allows a hint on the SMC structure before the last dynamical interaction with the LMC, which occurred about 200 Myr ago (Bekki & Chiba 2007). Better than an ellipsoidal distribution, the SMC old clusters follow an exponential-disk profile (Bica et al. 2008).

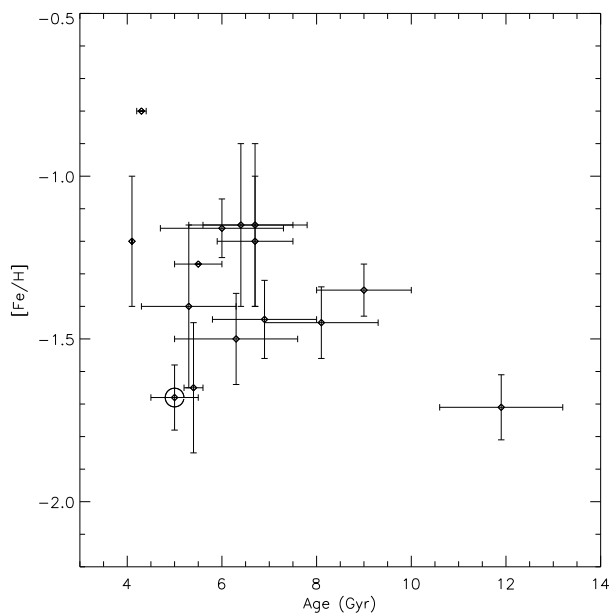
In Fig. 10 we present the SMC initial chemical enrichment determined by this population of old clusters. A comparison with the SMC chemical enrichment plot by Piatti et al. (2007) shows that BS 196 behaves like the rare metal-poor outlying cluster L 38 with similar age. BS 196 occupies the lower envelope of the distribution in Piatti et al. (2007). A fundamental question is whether lower mass clusters and/or their spatial distributions provide scatter effects in this plot. Larger samples are important to further probe that.

## 6 CONCLUSIONS

Since by now most of the populous old clusters in the SMC have been studied, we turned our attention to fainter clusters in similar environments. We carried out *B* and *V* photometry

**Table 2.** SMC clusters older than 4 Gyr.

| Designations                | $\alpha_{2000}$<br>(h:m:s) | $\delta_{2000}$<br>( $^{\circ}$ : ' : ") | age<br>(Gyr)   | [Fe/H]           | References           |
|-----------------------------|----------------------------|--|----------------|------------------|----------------------|
| AM-3, ESO28SC4              | 23:48:59                   | -72:56:43                                | $5.5 \pm 0.5$  | -1.27            | Da Costa (1999)      |
| L1, ESO28SC8                | 0:03:54                    | -73:28:19                                | $9.0 \pm 1.0$  | $-1.35 \pm 0.08$ | Crowl et al. (2001)  |
| L5, ESO28SC16               | 0:22:40                    | -75:04:29                                | 4.1            | $-1.2 \pm 0.2$   | Piatti et al. (2005) |
| K3, L8, ESO28SC19           | 0:24:47                    | -72:47:39                                | $6.0 \pm 1.3$  | $-1.16 \pm 0.09$ | Crowl et al. (2001)  |
| NGC121, K2, L10, ESO50SC12  | 0:26:47                    | -71:32:12                                | $11.9 \pm 1.3$ | $-1.71 \pm 0.10$ | Crowl et al. (2001)  |
| L32, ESO51SC2               | 0:47:24                    | -68:55:10                                | $6.7 \pm 0.8$  | $-1.2 \pm 0.2$   | Piatti et al. (2001) |
| L38, ESO51SC3               | 0:48:50                    | -69:52:11                                | $5.4 \pm 0.2$  | $-1.65 \pm 0.2$  | Piatti et al. (2001) |
| NGC339, K36, L59, ESO29SC25 | 0:57:42                    | -74:28:22                                | $6.3 \pm 1.3$  | $-1.50 \pm 0.14$ | Crowl et al. (2001)  |
| BS90                        | 0:59:06                    | -72:09:03                                | $4.3 \pm 0.1$  | -0.80            | Sabbi et al. (2007)  |
| NGC361, K46, L67, ESO51SC12 | 1:02:11                    | -71:36:21                                | $8.1 \pm 1.2$  | $-1.45 \pm 0.11$ | Crowl et al. (2001)  |
| NGC416, K59, L83, ESO29SC32 | 1:07:59                    | -72:21:20                                | $6.9 \pm 1.1$  | $-1.44 \pm 0.12$ | Crowl et al. (2001)  |
| L110, ESO29SC48             | 1:34:26                    | -72:52:28                                | $6.4 \pm 1.1$  | $-1.15 \pm 0.25$ | Piatti et al. (2007) |
| L112                        | 1:36:01                    | -75:27:28                                | $6.7 \pm 1.1$  | $-1.15 \pm 0.25$ | Piatti et al. (2007) |
| BS196                       | 1:48:02                    | -70:00:15                                | $5.0 \pm 0.5$  | $-1.68 \pm 0.10$ | this paper           |
| L113, ESO30SC4              | 1:49:28                    | -73:43:42                                | $5.3 \pm 1.0$  | $-1.40 \pm 0.25$ | Piatti et al. (2007) |

**Figure 10.** The early chemical enrichment of the SMC adapted from Piatti et al. (2007). BS 196 is indicated by a circle.

with the SOAR 4.1-m telescope of the outlying SMC star cluster BS 196. It is located in projection  $5.1^{\circ}$  (5.6 kpc) from the Northeast of the SMC optical centre, thus one of the farthest clusters from the main body.

We confirmed that BS 196 corresponds to the SMC distance modulus and it is thus not a far halo Galactic globular cluster. It is intrinsically faint with  $M_V = -1.89 \pm 0.39$ , a new class of objects to be explored. We derive an age of  $5.0 \pm 0.5$  Gyr and a metallicity  $[Fe/H] = -1.68 \pm 0.10$ . This lower mass cluster is at the lower envelope of values in the early chemical enrichment in the SMC.

This might suggest that some outer clusters share this property like L38 (Piatti et al. 2001). The cluster structure, fitted by 2 and 3 parameter King profiles, is well described by a core radius  $R_c = 2.66 \pm 0.14$  pc and a tidal radius

$R_t = 21.2 \pm 1.2$  pc. The cluster is rather loose with a concentration parameter  $c = 0.90$ .

The systematic study of such less populous clusters may reveal age gap clusters in the LMC, while in the SMC searches for faint additional genuine (by age) globular clusters are worth conducting to better understand the formation and evolution of star clusters in them. The knowledge of the early structure of the Clouds can also benefit from such studies.

## ACKNOWLEDGEMENTS

We thank L. Fraga and A. Roman-Lopes for the observations in service mode. JFCSJ thanks all SOAR members for making the observatory a pleasant environment to work during his stay in Chile as resident astronomer. We thank Dr. A. Piatti for providing information on his recent papers. This research used the facilities of the Canadian Astronomy Data Centre operated by the National Research Council of Canada with the support of the Canadian Space Agency. We acknowledge support from the Brazilian Institution CNPq.

## REFERENCES

- Banks T., Dodd R. J., Sullivan D. J., 1995, MNRAS, 274, 1225
- Bekki K., Chiba M., 2007, PASA, 24, 21
- Bica E., Bonatto C., 2008, MNRAS, 384, 1733
- Bica E., Bonatto C., Dutra C. M., Santos Jr. J. F. C., 2008, MNRAS, in press, 2008arXiv0806.3049
- Bica E., Dutra C. M., 2000, AJ, 119, 1214
- Bica E., Schmitt H. R., 1995, ApJS, 101, 41
- Burstein D., Heiles C., 1982, AJ, 87, 1165
- Crowl H. H., Sarajedini A., Piatti A. E., et al., 2001, AJ, 122, 220
- Da Costa G. S., 1999, in Y.-H. Chu, N. Suntzeff, J. Hesser, D. Bohlender, eds., IAU Symp. 190, New Views of the Magellanic Clouds, p. 446
- Girardi L., Bertelli G., Bressan A., et al., 2002, A&A, 391, 195

- Glatt K., Gallagher J. S., Grebel E. K. et al., 2008, preprint (astro-ph0801.1111)
- King I., 1962, *AJ*, 67, 471
- King I. 1966, *AJ*, 71, 64
- Hodge P. W., 1960, *ApJ*, 131, 351
- Mighell K. J., Sarajedini A., French R. S., 1998, *AJ*, 116, 2395
- Piatti A. E., Santos Jr. J. F. C., Clariá J. J., et al., 2001, *MNRAS*, 325, 792
- Piatti A. E., Sarajedini A., Geisler D., Bica E., Clariá J. J., 2002, *MNRAS*, 329, 556
- Piatti A. E., Sarajedini A., Geisler D. et al., 2005, *MNRAS*, 358, 1215
- Piatti A. E., Sarajedini A., Geisler D., Gallart C., Wischnjewsky M., 2007, *MNRAS*, 381, L84
- Rich R. M., Shara M., Fall S. M., Zurek D., 2000, *AJ*, 119, 197
- Sabbi E., Sirianni M., Nota A. et al., 2007, *AJ*, 133, 44
- Santos Jr. J. F. C., Bica E., Dottori H., 1990, *PASP*, 102, 454
- Schlegel D., Finkbeiner D., Davis M., 1998, *ApJ*, 500, 525
- Stetson P. B., 2000, *PASP*, 112, 925
- Tody D., 1993, in Hanisch R.J., Brissenden R.J.V., Barnes J., eds., *IRAF in the Nineties: Astronomical Data Analysis Software and Systems II*. Astron. Soc. Pac. Conference Ser., San Francisco, Vol. 52, 173
- Westerlund B. E., 1997, "The Magellanic Clouds", Cambridge Astrophysics Series #29, Cambridge Univ. Press.
- Yi S., Demarque P., Kim Y.-C., et al., 2001, *ApJS*, 136, 417